Constrained Iterative Technique With Embedded Neural Network for Dual-Polarization Radar Correction of Rain Path Attenuation

Gianfranco Vulpiani, Frank Silvio Marzano, *Senior Member, IEEE*, V. Chandrasekar, *Fellow, IEEE*, and Sanghun Lim

***Abstract*—A new stable backward iterative technique to correct for path attenuation and differential attenuation is presented here. The technique named, neural network iterative polarimetric precipitation estimator by radar (NIPPER), is based on a polarimetric model used to train an embedded neural network, constrained by the measurement of the differential phase along the rain path. Simulations are used to investigate the efficiency, accuracy, and the robustness of the proposed technique. The precipitation is characterized with respect to raindrop size, shape, and orientation distribution. The performance of NIPPER is evaluated by using simulated radar volumes scan generated from S-band radar measurements. A sensitivity analysis is performed in order to evaluate the expected errors of NIPPER. These evaluations show relatively better performance and robustness of the attenuation correction process when compared with currently available techniques.**

***Index Terms*—Attenuation correction, neural networks, polarimetric rain rate retrieval.**

I. Introduction

POLARIZATION diversity and agility of meteorological radar systems are important technological enhancements that have contributed to the improvement of rainfall microphysical characterization [1]. These techniques, proposed during the late seventies, have undergone a continuous progress [2]. Apart from a significant advantage in terms of data quality checks with respect to single-polarized radars, differential amplitude and phase features of the received signal can be exploited to estimate particle size, shape, orientation, and thermodynamic phase (e.g., [3] and [4]).

Polarimetric measurements are affected by typical errors of ground-based meteorological radars such as calibration, ground clutter, anomalous propagation, and beam blockage (e.g., [1]). For frequencies higher than S-band, path attenuation effects due to rainfall can become significant and need to be compensated for quantitative applications such as rainrate estimation [5]–[8].

Manuscript received February 27, 2005; revised July 7, 2005. This work was supported in part by the Italian Ministry of University and Research and in part by the Risk-AWARE INTERREG-IIIB CADSES Project and the U.S. National Science Foundation under Grant ERC-0313747.

G. Vulpiani is with Department of Electrical Engineering and also with CETEMPS, University of L'Aquila, 67040 L'Aquila, Italy (e-mail: g.vulpiani@aquila.infn.it).

F. S. Marzano is with the Department of Electronic Engineering, University of Rome "La Sapienza, "and also with with CETEMPS, University of L'Aquila, 67040 L'Aquila, Italy (e-mail: marzano@ing.univaq.it).

V. Chandrasekar and S. Lim are with Department of Electrical and Electronic Engineering, Colorado State University, Fort Collins, CO 80523 USA (e-mail: chandra@engr.colostate.edu).

Digital Object Identifier 10.1109/TGRS.2005.855623

Horizontally (H) and vertically (V) polarized microwaves propagating through precipitation are subject not only to back scattering and path attenuation, but also to differential phase shift and depolarization [9]–[11]. For single-polarized radar the iterative approaches to rain path attenuation correction, beginning from the first (closest to the radar) range resolution volume and proceeding forward to successive resolution volumes, are known to be unstable if path-integrated attenuation is relatively large [12]–[15]. In addition, these methods generally assume a power law relation between reflectivity and specific attenuation and an accurate calibration of the radar system. For polarimetric radars, algorithms using the specific differential phase are immune to such effects, but depend on the accuracy of its estimation [1], [9], [10]. The specific differential phase is the slope of the range profile of the differential phase, which can be estimated with an accuracy of at least few degrees within a range interval of the order of few kilometers [1].

A notable improvement to the design of path attenuation correction procedures has come from using the total path-integrated attenuation (PIA) as a constraint. One of the proposed approaches to estimate PIA, complementing the Hitschfeld–Bordan method [16], is the surface reference technique (SRT), which was developed for spaceborne weather radar [17]–[24]. Dual-polarized radars can provide the estimate of path-integrated attenuation using the total differential propagation phase because specific attenuation and specific differential phase are almost linearly related at typical ground-based radar frequency bands (S, C, and X) [9]. Starting from this paradigm, the use of the differential phase constraint to correct the measured reflectivity and differential reflectivity, proposed and evaluated in [6] and [7] respectively, was improved in [8] through the use of a self-consistent scheme. One of the problems with the differential phase constraint method is the requirement to assume that the intercept parameter N_w of the underlying drop size distribution along the precipitation path is constant.

The aim of this paper is to introduce a new approach for attenuation correction with the differential phase, used as a constraint, to retrieve both horizontal reflectivity and differential reflectivity at C-band. The suggested technique, named neural network iterative polarimetric precipitation estimator by radar (NIPPER), is based on a backward iterative estimation of specific attenuation and differential attenuation starting from the farthest range volume. The principle behind this procedure is to merge the strengths of the iterative approaches, namely their flexibility and ability to ingest advanced estimation techniques, with some features of the self-consistent rain-profiling

0196-2892/$20.00 © 2005 IEEE

approaches. From the farthest range volume to the closest one, copolar and differential path attenuation are estimated using the preceding range volume values of differential phase, corrected copolar reflectivity and differential reflectivity using a feedforward neural network (NN) with a backpropagation learning algorithm [27], [28]. The performance of the proposed method is evaluated by using a simulated radar field generated from S-band radar measurements.

The paper is organized as follows. After a description of the theoretical background of the rain model in Section II, an illustration of the rain profiling algorithms for attenuation correction and a description of the proposed new technique are given in Section III. In Section IV, the performance of the attenuation correction techniques is examined.

II. Rain Model

Microphysical properties of the rain medium can be described by the size, shape, and orientation distributions. The following paragraphs briefly describe the raindrop size and shape distribution assumed within the context of this work.

A. Raindrop Size Distribution and Axis Ratio Model

A Gamma raindrop size distribution (RSD), having the general form $N(D) = N_0 D^{\mu}\exp(-\Lambda D)$ with D the particle diameter and N_0, μ, and Λ RSD parameters, has been introduced in literature to account for most of the variability occurring in the naturally observed size distributions [1], [29].

The multiplication constant N_0, whose units are μ-dependent (i.e., [mm$^{-1-\mu}\cdot$m^{-3}]), is not physically meaningful when $\mu \neq 0$. In order to study the underlying shape of the RSD for widely varying rainfall rates, the concept of RSD normalization has been introduced in [31] and revisited in [32]–[34]. The normalized Gamma RSD can be written as [1]

$$N(D) = N_w f(\mu)\left(\frac{D}{D_0}\right)^{\mu}\exp\left[-(3.67+\mu)\frac{D}{D_0}\right] \quad (1)$$

where the parameter D_0 [mm] is the median volume drop diameter, μ is the shape of the drop spectrum, and N_w [mm$^{-1}\cdot$ m^{-3}] is the normalized drop concentration that can be calculated as a function of liquid water content W [g$\cdot$m $^{-3}$] and D_0 (e.g., [1]). The function $f(\mu)$ is a function of μ only defined by

$$f(\mu) = \frac{6}{(3.67)^4}\frac{(3.67+\mu)^{\mu+4}}{\Gamma(\mu+4)}. \quad (2)$$

The shape of a raindrop can be described by an oblate spheroid. The relation between the equivalent spherical volume diameter D [mm] and the raindrop axis ratio r_a (i.e., ratio between the drop minor and major axis) has been investigated by several authors. In this study we assumed the relationship proposed in [35], i.e.,

$$r_a = 0.005 + 10^{-4}(5.7D - 260D^2 + 37D^3 - 2D^4). \quad (3)$$

A raindrop falls with its symmetry axis aligned in the vertical direction. The canting angle in the polarization plane is defined as the angle measured clockwise between the projection of the symmetry axis of spheroidal particle and the direction running opposite to the vertical one. Consequently, in case of horizontal incidence it coincides with the tilt of the particle symmetry axis (e.g., [1]). As shown in [36], the distribution of canting angles can be represented by a Gaussian model with zero mean and standard deviation $\leq 5^{\circ}$.

B. Polarimetric Radar Observables

This section describes numerical computations of polarimetric variables for rainfall carried out for the 5-cm wavelength. A Gamma distribution has been assumed for drop diameters between $D_1 = 0.5$ and $D_2 = 8$ mm. At C-band wavelength, the transition between Rayleigh and Mie scattering occurs for water drops of about 3 to 4 mm. The extension into the resonant scattering region needs use of accurate numerical solution, such as the T-matrix method, to describe the scattering properties of raindrops and compute the scattering amplitude matrix $\boldsymbol{S}$ [mm^2] [37]–[39].

The rainfall rate R [mm$\cdot$h^{-1}] and the radar reflectivity factors $Z_{\rm hh,vv}$ [mm $^6\cdot$m^{-3}] at horizontal and vertical polarization, respectively, can be expressed in terms of ensemble average over the RSD as follows:

$$R = 0.6\pi 10^{-3}\int_{D_1}^{D_2} D^3 N(D) v(D) dD \quad (4)$$

$$Z_{\rm hh,vv} = \frac{\lambda^4}{\pi^5 |K|^2}\int_{D_1}^{D_2} 4\pi |S_{\rm hh,vv}(D)|^2 N(D) dD \quad (5)$$

where D_1 and D_2 are the minimum and maximum drop diameters, respectively, $S_{\rm hh,vv}$ are the backscattering copolar components of $\boldsymbol{S}$ at H and V polarization, respectively, and λ is the wavelength. K is a constant defined as $K = (\varepsilon - 1)/(\varepsilon + 2)$ where ε is the complex dielectric constant of water estimated as a function of wavelength and temperature [40]. Finally, $v(D)$ is the terminal fall speed in still air. As derived in [41], the $v(D)$ can be expressed using the following relationship:

$$v(D) = 3.67 D^{0.67}. \quad (6)$$

Among the most important observables of a polarimetric radar, the differential reflectivity $Z_{\rm dr}$ plays a relevant role. It is defined as the ratio of reflectivity factors at two orthogonal polarizations, i.e.,

$$Z_{\rm dr} = \frac{Z_{\rm hh}}{Z_{\rm vv}}. \quad (7)$$

The specific differential phase shift $K_{\rm dp}$ [$^{\circ}\cdot$km^{-1}], which is due to the propagation phase difference between the two orthogonal polarizations, the specific power attenuation $\alpha_{\rm hh,vv}$ [dB $\cdot$ km^{-1}], and the copolar correlation coefficients $\rho_{\rm hv}$ can be also obtained in terms of the scattering matrix $\mathbf{S}$ as well as the forward copolar scattering amplitudes $f_{\rm hh}$ and $f_{\rm vv}$ as

$$K_{\rm dp} = 10^{-3}\frac{180}{\pi}\lambda\,{\rm Re}\int_{D_1}^{D_2}[f_{\rm hh}(D) - f_{\rm vv}(D)]N(D)dD \quad (8)$$

$$\alpha_{\rm hh,vv} = 8.686\times 10^{-3}\lambda\,{\rm Im}\int_{D_1}^{D_2} f_{\rm hh,vv}(D)N(D)dD \quad (9)$$

$$\rho_{\rm hv} = \frac{\int_{D_1}^{D_2} S_{\rm vv}(D)S_{\rm hh}^{*}(D)N(D)dD}{\sqrt{\int_{D_1}^{D_2}|S_{\rm hh}(D)|^2 N(D)dD\int_{D_1}^{D_2}|S_{\rm vv}(D)|^2 N(D)dD}} = |\rho_{\rm hv}|e^{j\delta_{\rm hv}} \quad (10)$$

where λ [m] and $\delta_{\rm hv}[^\circ]$ is the backscattering differential phase shift.

C. Randomly Generated Training Dataset

The proposed algorithm has been trained using polarimetric radar variables simulated using RSD parameters randomly and independently varying in the following wide ranges [42], [43]:

$$10^3 \le N_w \le 10^5\ [\text{mm}^{-1}\cdot\text{m}^{-3}] \tag{11a}$$
$$0.5 \le D_0 \le 3.5\ [\text{mm}] \tag{11b}$$
$$-1 < \mu \le 4. \tag{11c}$$

Moreover, the temperature (impacting the dielectric constant) has been varied between 5 °C and 30 °C. The dataset is limited to rainfall values up to 300 mm $\cdot$ h^{-1} and $Z_{\rm hh}$ up to 60 dBZ.

Finally, a zero-mean random fluctuation of polarimetric variables has been introduced to realistically reproduce the measurables, resulting in a noise standard deviation of 1 dB for $Z_{\rm hh}$, 0.3 dB for $Z_{\rm dr}$, and 2° for $\Phi_{\rm dp}$ [1].

III. Constrained Polarimetric Techniques

The rain profiling algorithms were originally developed for spaceborne radar operating at frequencies greater than 10 GHz [17]–[24]. In Section III-A, we briefly describe the rain profiling algorithm for ground-based radar (named ZPHI) [6]. The basic principles of the ZPHI method is presented in order to better highlight the underlying assumptions and to prepare the background for the proposed iterative approach, described in Section III-B.

In presence of path attenuation, the measured copolar reflectivity $Z^m_{\rm hh}$ [mm$^6\cdot$m^{-3}] and differential reflectivity $Z^m_{\rm dr}$ can be written, as [1], [29]

$$10\log_{10}\left(Z^m_{\rm hh}(r)\right) = 10\log_{10}(Z_{\rm hh}(r)) - 2A_{\rm hh}(r_0,r) \tag{12a}$$
$$10\log_{10}\left(Z^m_{\rm dr}(r)\right) = 10\log_{10}(Z_{\rm dr}(r)) - 2A_{\rm dp}(r_0,r) \tag{12b}$$

where r is the range and r_0 is the rain range bin closest to the radar or, in general, the initial range of the considered rain segment. The one-way copolar $A_{\rm hh}$ and differential $A_{\rm dp}$ path attenuation factors are defined as

$$A_{\rm hh}(r_0,r) = \int_{r_0}^{r} \alpha_{\rm hh}(s)\,ds \tag{13a}$$
$$A_{\rm dp}(r_0,r) = \int_{r_0}^{r} \alpha_{\rm dp}(s)\,ds = \int_{r_0}^{r} [\alpha_{\rm hh}(s) - \alpha_{\rm vv}(s)]\,ds \tag{13b}$$

where s is the range variable. From (12), it is evident that path attenuation correction is critically important to retrieve intrinsic $Z_{\rm hh}$ and $Z_{\rm dr}$.

A. Rain Profiling Method for Path Attenuation Correction

In order to solve (12), a further relation can be introduced to simplify the inverse problem. The copolar specific attenuation $\alpha_{\rm hh}$ [dB $\cdot$ km^{-1}] can be parameterized to be related to $Z_{\rm hh}$ through a power law

$$\alpha_{\rm hh}(r) = a(r)[Z_{\rm hh}(r)]^{b(r)}. \tag{14}$$

Assuming that b is constant along the range, (12) can be rewritten as a differential equation (e.g., [22]) which takes the form of a Riccati differential equation [44, Sec. 10.3]. A general solution to this differential equation is

$$\alpha_{\rm hh}(r) = a(r)\,[Z^m_{\rm hh}(r)]^b\,[C - S^m_{\rm hh}(r_0,r)]^{-1} \tag{15a}$$

where C is the integration constant and

$$S^m_{\rm hh}(r_0,r) = 2b\int_{r_0}^{r} a(s)\,[Z^m_{\rm hh}(s)]^b\,ds. \tag{15b}$$

It is worth mentioning that the same approach can be followed to derive the specific differential attenuation $A_{\rm dp}$ as a function of differential reflectivity $Z_{\rm dr}$.

If $Z_{\rm hh}(r_0) = Z^m_{\rm hh}(r_0)$ at $r = r_0$ is taken as a boundary condition, then the Hitschfeld–Bordan solution is obtained [16]. In order to avoid the instability of the solution, the boundary condition at the farthest range bin can be applied to constrain the solution.

The rain profiling method, as applied to ground radars, uses measurements of the two-way differential phase shift $\Phi_{\rm dp}$ to estimate the path-integrated attenuation and constrain the analytical solution [6]. The incremental $\Phi_{\rm dp}$ between r_0 and r_N is defined as

$$\Delta\Phi_{\rm dp}(r_0,r_N) = 2\int_{r_0}^{r_N} K_{\rm dp}(s)\,ds = \Phi_{\rm dp}(r_N) - \Phi_{\rm dp}(r_0). \tag{16}$$

It has been proposed that $\alpha_{\rm hh}$ and $\alpha_{\rm dp}$ [dB$\cdot$km^{-1}] are linearly related to $K_{\rm dp}$ [$^\circ\cdot$ km^{-1}]

$$\alpha_{\rm hh}(r) = \gamma_1 K_{\rm dp}(r) \tag{17a}$$
$$\alpha_{\rm dp}(r) = \gamma_2 K_{\rm dp}(r) \tag{17b}$$

where γ_1 and γ_2 are frequency-dependent and temperature-sensitive parameters. $K_{\rm dp}$ may be retrieved from $\Phi_{\rm dp}$ over a given range interval [1]. Note that before estimating $K_{\rm dp}$, the measured differential phase shift needs to be filtered in order to remove the backscattering component $\delta_{\rm hv}$ [1], [6], [8]. As a consequence, an estimate of the path-integrated attenuation $A_{\rm hh}$ [dB] at the farthest range r_N, through (16) and (17), is

$$\hat{A}_{\rm hh}(r_0,r_N) = \int_{r_0}^{r_N} \alpha_{\rm hh}(s)\,ds = \frac{\gamma_1}{2}\Delta\Phi^f_{\rm dp}(r_0,r_N) \tag{18}$$

where the "^" indicates an estimated quantity, and $\Phi^f_{\rm dp}$ is the filtered differential phase shift. Analogously, $A_{\rm dp}$ can be estimated from (18) by simply substituting γ_1 with γ_2.

Based on the theory of normalized RSD, it can be shown that a is related to N_w, and b is constant [1], [33]. Under this condition the solution to the specific attenuation is obtained as

$$\hat{\alpha}_{\rm hh}(r) = \frac{[Z^m_{\rm hh}(r)]^b\left[10^{0.2b\hat{\rm A}_{\rm hh}(r_0,r_N)} - 1\right]}{I^m_{\rm hh}(r_0,r) + \left(10^{0.2b\hat{\rm A}_{\rm hh}(r_0,r_N)} - 1\right) I^m_{\rm hh}(r,r_N)} \tag{19}$$

where $I^m_{\rm hh} = S^m_{\rm hh}/a$. Note that the last equality is true only if $a(r)$ is constant with respect to r. The same considerations apply to the estimate of $\alpha_{\rm dp}$ through (19) using $A_{\rm dp}$.

Within the rain profiling approach, the coefficient γ_1 is assumed to be known though it depends on temperature [25]. This assumption generally leads to errors in the estimation of $A_{\rm hh,dp}$ affecting the attenuation correction procedure. To overcome this problem the self-consistent solution was proposed in [8] (named self-consistent ZPHI). This approach is able to adjust the coefficients γ_1 and γ_2 so that the integrated retrieved attenuation and differential attenuation profiles are consistent with the measured $\Phi_{\rm dp}$ profile. The optimal value is found by minimizing, with respect to γ_1, the following objective function:

$$J(\gamma_1) = \int_{r_0}^{r_N} \left| \Delta\Phi^f_{\rm dp}(r_0, r) - \frac{2}{\gamma_1} \int_{r_0}^{r} \hat{\alpha}_{\rm hh}(s)\, ds \right| dr \qquad (20)$$

The self-consistent method also improves the $Z_{\rm dr}$ correction algorithm described in [5] by optimizing the coefficient γ_2.

Subsequently, the estimate of $\alpha_{\rm hh}$ and $\alpha_{\rm dp}$ are obtained through (19); by inverting (12) the corresponding corrected reflectivities can be then derived

$$10\log_{10}(\hat{Z}_{\rm hh}(r)) = 10\log_{10}\left(Z^m_{\rm hh}(r)\right) + 2\hat{A}_{\rm hh}(r_0, r) \qquad (21a)$$

$$10\log_{10}(\hat{Z}_{\rm dr}(r)) = 10\log_{10}\left(Z^m_{\rm dr}(r)\right) + 2\hat{A}_{\rm dp}(r_0, r). \qquad (21b)$$

B. Constrained Iterative Technique

Iterative techniques for correcting rain path attenuation are known to be highly unstable when the total attenuation exceeds few decibels, a relatively common case for intense rainfall at C-band and beyond [45]–[47]. In this paper, the iterative procedure is combined synergistically with new estimation methodology, using neural networks. The philosophy behind a hybrid approach is to merge the advantage of polarimetric radar measurements to constrain the inverse problem, as done by the self-consistent technique, within an iterative numerical solution [43].

The methodology of NIPPER is described in Fig. 1. The proposed backward iterative algorithm is based on partitioning the profile variability to $N+1$ contiguous range bins. If r_i with $i = 0, \ldots, N$ represents the center range value of each bin, from (12) we have

$$10\log_{10}\left(Z^m_{\rm hh}(r_i)\right) = 10\log_{10}(Z_{\rm hh}(r_i)) - 2A_{\rm hh}(r_0, r_i), \quad i = 0, \ldots, N \qquad (22a)$$

$$10\log_{10}\left(Z^m_{\rm dr}(r_i)\right) = 10\log_{10}(Z_{\rm dr}(r_i)) - 2A_{\rm dp}(r_0, r_i), \quad i = 0, \ldots, N \qquad (22b)$$

where r_0 and r_N are the first and the last ranges. Subsequently (13) can be written as a discrete sum to be

$$A_{\rm hh}(r_0, r_i) = \sum_{i=0}^{N} \alpha_{\rm hh}(r_i)\Delta r \qquad (23a)$$

$$A_{\rm dp}(r_0, r_i) = \sum_{i=0}^{N} [\alpha_{\rm hh}(r_i) - \alpha_{\rm vv}(r_i)]\Delta r. \qquad (23b)$$

The first step of NIPPER is the estimation of the path-integrated attenuation $A_{\rm hh}(r_0, r_N)$ and differential attenuation $A_{\rm dp}(r_0, r_N)$ at the range r_{N-1} from the filtered measurement of $\Delta\Phi^f_{\rm dp}(r_0, r_N)$ by using (18). The corrected values of $Z_{\rm hh}$ and $Z_{\rm dr}$ are then derived at the farthest range volume r_N by inverting (22), i.e.,

$$10\log_{10}(\hat{Z}_{\rm hh}(r_N)) = 10\log_{10}\left(Z^m_{\rm hh}(r_N)\right) + \gamma_1 \left[\Delta\Phi^f_{\rm dp}(r_0, r_N)\right] \qquad (24a)$$

$$10\log_{10}(\hat{Z}_{\rm dr}(r_N)) = 10\log_{10}\left(Z^m_{\rm dr}(r_N)\right) + \gamma_2 \left[\Delta\Phi^f_{\rm dp}(r_0, r_N)\right]. \qquad (24b)$$

Using the corrected (estimated) values of $Z_{\rm hh}(r_N)$ and $Z_{\rm dr}(r_N)$, it is possible to estimate the specific attenuation and specific differential attenuation at the Nth range volume by means of

$$\hat{\alpha}_{\rm hh}(r_N) = NN_{\rm hh}\{10\log_{10}(\hat{Z}_{\rm hh}(r_N)), 10\log_{10}(\hat{Z}_{\rm dr}(r_N))\} \qquad (25a)$$

$$\hat{\alpha}_{\rm dp}(r_N) = NN_{\rm dp}\{10\log_{10}(\hat{Z}_{\rm hh}(r_N)), 10\log_{10}(\hat{Z}_{\rm dr}(r_N))\} \qquad (25b)$$

where $\rm NN_{hh,dp}$ represent the neural network functional blocks used for $\alpha_{\rm hh}$ and $\alpha_{\rm dp}$ estimation, respectively.

Neural networks represent a powerful tool for nonlinear inverse problems, and they have been already applied to rainrate estimation from radar data (e.g., [1] and [27]). A topology with an input, a hidden, and an output layer is shown to approximate a nonlinear function to any degree of nonlinearity [48]. A multilayer feedforward neural network, characterized by a backpropagation learning rule, an input layer, and an output layer, was implemented in this work. A four-layer neural network, composed by an input layer, two hidden layers, and an output layer, was chosen for its simplicity and effectiveness. The number of input nodes was set to two, while the number of output nodes to 1. After an optimization process, called "neural network pruning," the number of nodes in the hidden layers was chosen equal to 4 and 3, respectively. The dataset for training the NNs in (25) was that described in Section II-C.

Using this approach, from (23) we can estimate $A_{\rm hh,dp}$ at the $(N-1)$th range bin through

$$\hat{A}_{\rm hh}(r_0, r_{N-1}) = \hat{A}_{\rm hh}(r_0, r_N) - \hat{\alpha}_{\rm hh}(r_N)\Delta r \qquad (26a)$$

$$\hat{A}_{\rm dp}(r_0, r_{N-1}) = \hat{A}_{\rm dp}(r_0, r_N) - \hat{\alpha}_{\rm dp}(r_N)\Delta r \qquad (26b)$$

where Δr is the range bin resolution where the specific attenuation is assumed to be constant. From (22) the corrected values of reflectivity and differential reflectivity are

$$10\log_{10}(\hat{Z}_{\rm hh}(r_{N-1})) = 10\log_{10}\left(Z^m_{\rm hh}(r_{N-1})\right) + 2\hat{A}_{\rm hh}(r_0, r_{N-1}) \qquad (27a)$$

$$10\log_{10}(\hat{Z}_{\rm dr}(r_{N-1})) = 10\log_{10}\left(Z^m_{\rm dr}(r_{N-1})\right) + 2\hat{A}_{\rm dp}(r_0, r_{N-1}). \qquad (27b)$$

Generalizing previous equations, we can write the following set of iterative equations whose initialization for $k = N$ (farthest range from the radar) is given by

$$\hat{A}_{\rm hh}(r_0, r_N) = \frac{\gamma_1}{2}\Delta\Phi^f_{\rm dp}(r_0, r_N)$$

$$\hat{A}_{\rm dp}(r_0, r_N) = \frac{\gamma_2}{2}\Delta\Phi^f_{\rm dp}(r_0, r_N) \qquad (28a)$$

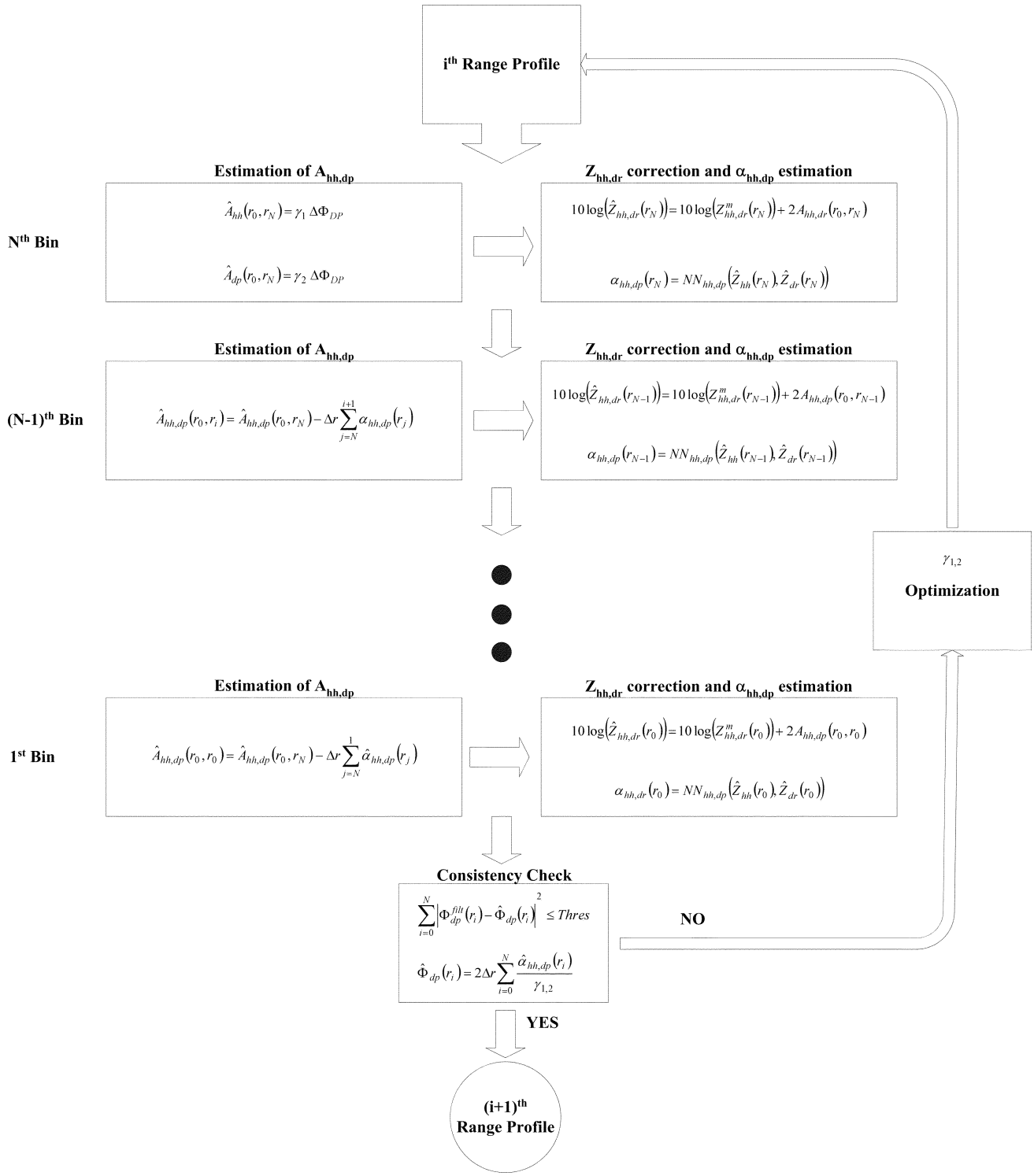

Fig. 1. Block diagram of the proposed attenuation correction technique.

$$10\log_{10}(\hat{Z}_{\rm hh}(r_N)) = 10\log_{10}(Z^m_{\rm hh}(r_N)) + 2\hat{A}_{\rm hh}(r_0,r_N)$$
$$10\log_{10}(\hat{Z}_{\rm dr}(r_N)) = 10\log_{10}(Z^m_{\rm dr}(r_N)) + 2\hat{A}_{\rm dp}(r_0,r_N). \quad (28b)$$

With i varying from $N-1$ to 0 (closest range to the radar) it holds

$$\hat{\alpha}_{\rm hh}(r_i) = NN_{\rm hh}\{10\log_{10}(\hat{Z}_{\rm hh}(r_i)), 10\log_{10}(\hat{Z}_{\rm dr}(r_i))\}$$
$$\hat{\alpha}_{\rm dp}(r_i) = NN_{\rm dp}\{10\log_{10}(\hat{Z}_{\rm hh}(r_i)), 10\log_{10}(\hat{Z}_{\rm dr}(r_i))\} \quad (28c)$$

$$\hat{A}_{\rm hh}(r_0,r_i) = \hat{A}_{\rm hh}(r_0,r_N) - \Delta r\sum_{j=N}^{i+1}\hat{\alpha}_{\rm hh}(r_j)$$
$$\hat{A}_{\rm dp}(r_0,r_i) = \hat{A}_{\rm dp}(r_0,r_N) - \Delta r\sum_{j=N}^{i+1}\hat{\alpha}_{\rm dp}(r_j) \quad (28d)$$

$$10\log_{10}(\hat{Z}_{\rm hh}(r_i)) = 10\log_{10}(Z^m_{\rm hh}(r_i)) + 2\hat{A}_{\rm hh}(r_0,r_i)$$
$$10\log_{10}(\hat{Z}_{\rm dr}(r_i)) = 10\log_{10}(Z^m_{\rm dr}(r_i)) + 2\hat{A}_{\rm dp}(r_0,r_i). \quad (28e)$$

At the end of this process, a minimization step is also accomplished in order to optimize the value of γ_1 and γ_2. A slightly different objective function is used resorting to the maximum-likelihood approach (e.g., [49]), i.e.,

$$J = \sum_{i=1}^{N} \left\{ \frac{1}{\sigma_\alpha^2} \left[\Delta\Phi_{\rm dp}^f(r_0, r_i) - \frac{2}{\gamma_1} \Delta r \sum_{j=0}^{i} \hat{\alpha}_{\rm hh}(r_j) \right]^2 + \frac{1}{\sigma_\beta^2} \left[\Delta\Phi_{\rm dp}^f(r_0, r_i) - \frac{2}{\gamma_2} \Delta r \sum_{j=0}^{i} \hat{\alpha}_{\rm dp}(r_j) \right]^2 \right\} \quad (29)$$

where σ_α and σ_β are the standard deviations of γ_1 and γ_2 terms in (29), to be used as weights for balancing the confidence in the copolar and differential estimated attenuation. In this work, we have set σ_α equal to σ_β. It is worth mentioning that a coupled minimization procedure has been applied to find the optimal values of γ_1 and γ_2. In fact, $\alpha_{\rm hh}$ and $\alpha_{\rm dp}$ are estimated both from the corrected values of $Z_{\rm hh}$ and $Z_{\rm dr}$ using distinct NNs. Consequently, the terms in (29) are not completely independent.

Moreover, a test on $\delta_{\rm hv}$ is also performed by estimating the latter from the corrected values of $Z_{\rm hh}$ and $Z_{\rm dr}$ using another neural network algorithm

$$\hat{\delta}_{\rm hv}(r_i) = NN_\delta\{\hat{Z}_{\rm hh}(r_i), \hat{Z}_{\rm dr}(r_i)\} \quad (30)$$

where $\rm NN_\delta$ represents the neural network functional block used for $\delta_{\rm hv}$ estimation.

The performance of the NN-based estimator in (30) is usually better than that of a polynomial regression based on $Z_{\rm dr}$ only [28]. Finally, if J is less than a given threshold and $\delta_{\rm hv}$ is less than a given value (set to 2° by default), than the process is stopped; otherwise the previous equation set is iterated again.

The proposed correction algorithm is the implementation of (28)–(30) so that it is possible to iteratively correct the profiles of $Z_{\rm hh}$ and $Z_{\rm dr}$ in a stable and robust manner.

IV. Numerical Results

This section describes the evaluation of the NIPPER algorithm.

A. S-Band-Derived Test Dataset

The dataset used to test the proposed algorithm has been simulated adopting the rain model specified in Section II-A where the RSD parameters have been retrieved from S-band radar measurements. Adopting the procedure proposed in [4], the polarimetric variables $Z_{\rm hh}^m, Z_{\rm dr}^m$, and $K_{\rm dp}^m$, measured by the CSU-CHILL radar during a convective event, have been used to estimate the drop median parameter D_0 and the intercept parameter N_w.

Radar measurements have been performed choosing a pulse repetition frequency (PRF) and a pulsewidth such that the maximum unambiguous range is about 80 km and the range resolution is 250 m.

Fixing the temperature and consequently the relative dielectric constant, a complete volume scan at C-band has been simulated.

A random noise on simulated polarimetric variables has been introduced to realistically reproduce the measurements [6], resulting in a 1-dB fluctuation for $Z_{\rm hh}$, 0.3 dB for $Z_{\rm dr}$, and 2° for $\Phi_{\rm dp}$.

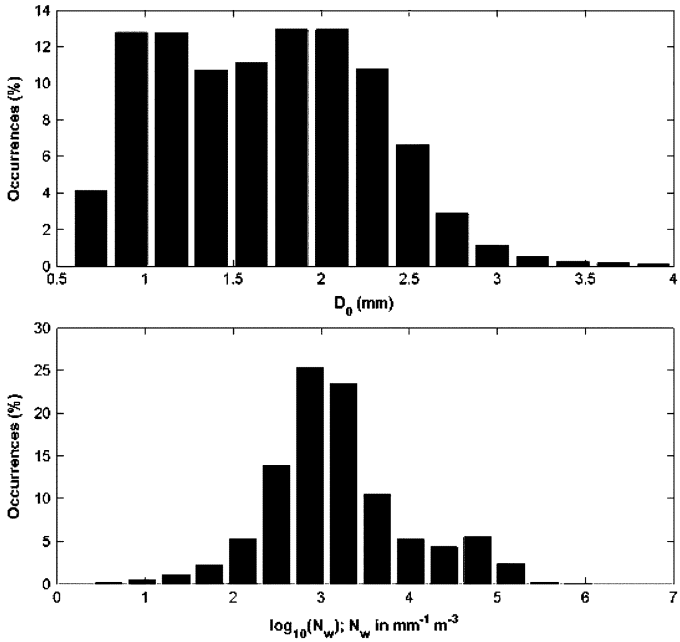

Fig. 2. Histogram of the raindrop size distribution parameters.

Fig. 2 shows the histograms of D_0 and N_w encountered in the dataset. The range of variability of the median volume diameter is $0.5 \leq D_0 \leq 3.5$ mm (about 99.6% of the cases), while that one relative to the normalized drop concentration is $10^2 \leq N_w \leq 10^5 \cdot \rm m^{-3} \cdot mm \cdot ^{-1}$ (about 93% of the cases).

The plan position indicators (PPIs) of the reflectivity and differential reflectivity are shown in Fig. 3. The intensity of $Z_{\rm hh}$ and $Z_{\rm dr}$ highlights the presence of wide convective areas and stratiform regions. Fig. 4 shows the two-way path-integrated attenuation as a function of the azimuth. About 50% of rays have a PIA greater than 2 dB. The most attenuated rays are localized in the sectors $70° \leq \varphi \leq 90°$ and $145° \leq \varphi \leq 160°$, where φ is the azimuth angle, with a maximum two-way PIA up to 10 dB.

B. Error Budget of Attenuation Correction

The results obtained by applying the proposed attenuation compensation technique to the simulated dataset are here examined assuming a well-calibrated radar. The evaluation of system bias impact is described in the next Section IV-C.

The performance of NIPPER is evaluated in terms of error mean value ($\bar{\varepsilon}_{\rm hh,dr}$) and its standard deviation ($\sigma(\varepsilon_{\rm hh,dr})$), computed as a function of range and for all azimuth profiles. In this work the error is defined as

$$\varepsilon_{\rm hh,dr}(r) = 10\log_{10}(\hat{Z}_{\rm hh,dr}(r)) - 10\log_{10}(Z_{\rm hh,dr}(r)) \quad (31)$$

where $\hat{Z}_{\rm hh,dr}$ indicates the estimate of the attenuation-corrected radar reflectivity. Figs. 5 and 6 show the plot of $\bar{\varepsilon}_{\rm hh,dr}$ and $\sigma(\varepsilon_{\rm hh,dr})$, the metrics of the copolar reflectivity and differential reflectivity retrieval, as a function of the azimuth for both the self-consistent ZPHI and NIPPER algorithms.

It can be seen from Fig. 5 that the proposed attenuation compensation procedure is characterized by a considerable improvement with respect to the self-consistent rain profiling algorithm. This behavior is more evident when the attenuation is relatively

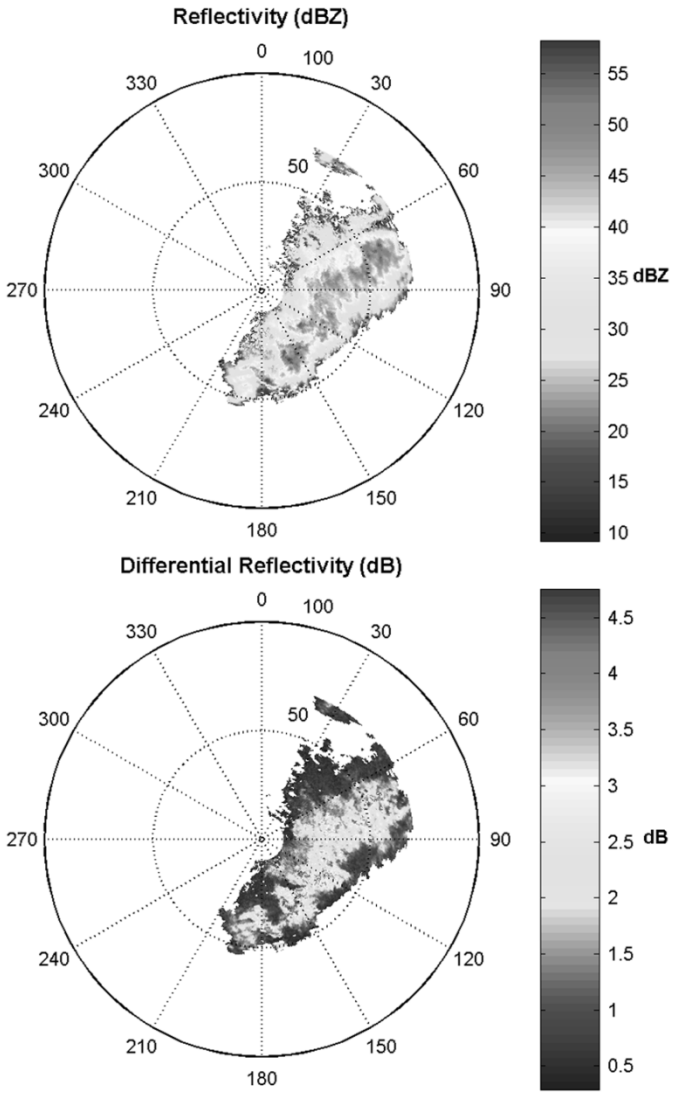

Fig. 3. PPI of (upper panel) the synthetic apparent reflectivity and (lower panel) differential reflectivity.

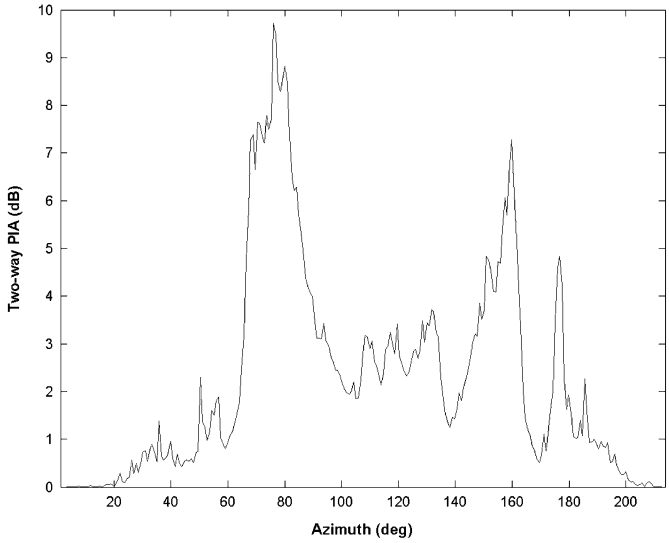

Fig. 4. Two-way PIA as function of the azimuth.

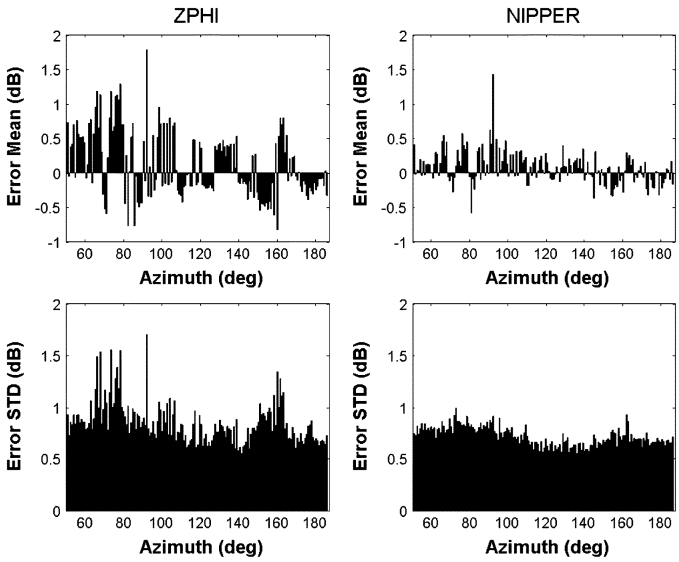

Fig. 5. Reflectivity retrieval. (Right panels) The NIPPER performance (right panels) is compared with the rain profiling algorithm one (left panels) in case of well-calibrated radar.

high (see Fig. 4). If all the processed rays are considered, 78.7% have a mean error less than 0.5 dBZ and a standard deviation less than 0.8 dBZ. Using the self-consistent rain profiling algorithm, the same values of $\bar{\varepsilon}$ and σ_{ε} are obtained in 43.7% of the cases.

Similarly, the differential reflectivity has been corrected (see Fig. 6) with a mean error less than 0.2 and a standard deviation less than 0.3 for 79.3% of all rays by NIPPER and 52.1% by the self-consistent rain profiling algorithm.

C. Impact of System Bias

Systematic errors on $Z_{\rm hh}$ and $Z_{\rm dr}$ can affect both the attenuation compensation and the rainfall retrieval algorithms. Typically, in a well-maintained radar the error bias on $Z_{\rm dr}$ is less than 0.2 dB, while the bias on $Z_{\rm hh}$ is less than 1 dBZ. The bias on differential reflectivity can be estimated and removed in a fairly easy way [47], because it is a differential power measurement. However, it is difficult to obtain the absolute calibration of $Z_{\rm hh}$. For this reason, assuming a bias of 0.2 dB on $Z_{\rm dr}$, we focused on the impact that the error bias on $Z_{\rm hh}$ has on the path attenuation correction technique.

The impact of system bias on path attenuation and differential attenuation correction are evaluated in Figs. 7 and 8, again in terms of the mean and the standard deviation of the error. As shown in Figs. 7 and 8, both the self-consistent rain profiling algorithm and NIPPER are sensitive to radar calibration. In this case, we have found an increase of both $|\bar{\varepsilon}|$ and σ_{ε}. As shown in Fig. 7, using the proposed iterative technique, about 82% of the corrected profiles of reflectivity are affected by a mean error less than 1.5 dBZ and a standard deviation less than 1 dBZ. On the contrary, using the self-consistent rain profiling algorithm, we found that about 70% of the reflectivity profiles are characterized by the same values of $|\bar{\varepsilon}|$ and σ_{ε}. It can be seen, from Fig. 8, that the differential reflectivity has been corrected with a mean error less than 0.4 and a standard deviation less than 0.35 in 84% of the rays by NIPPER and 69% by the self-consistent rain profiling algorithm.

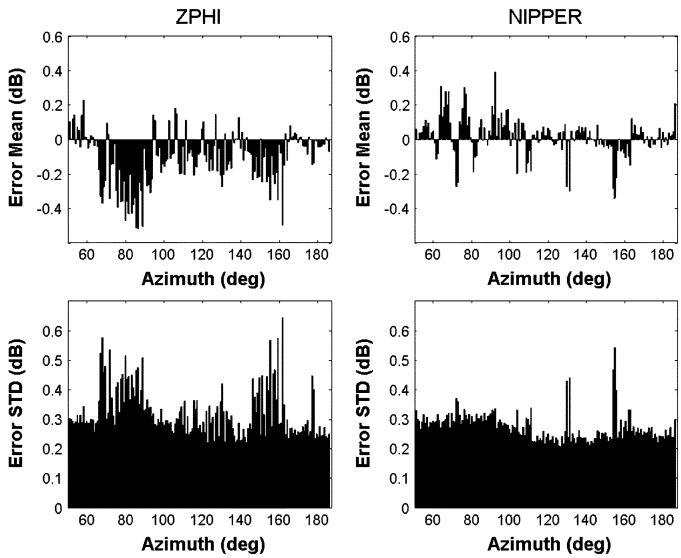

Fig. 6. Differential reflectivity retrieval. The NIPPER performance (right panels) is compared with the rain profiling algorithm one (left panels) in case of well-calibrated radar.

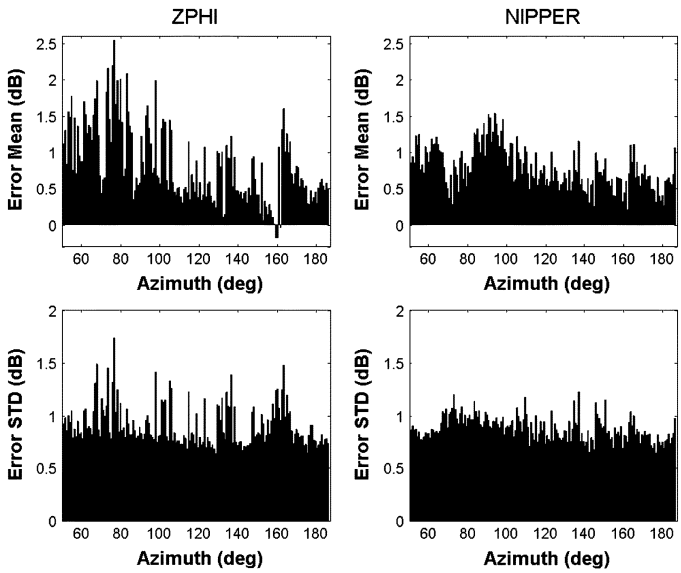

Fig. 7. Reflectivity retrieval. The NIPPER performance (right panels) is compared with the rain profiling algorithm one (left panels) in presence of system bias (1 dBZ on Z_{hh} and 0.2 dB on Z_{dr}).

V. Summary and Conclusion

Dual-polarization radar measurements can be significantly affected by rain path attenuation, especially for moderate to intense precipitation intensity. This effect is one of the important error sources that need to be compensated before using radar data for quantitative applications, especially for C-band systems.

Iterative techniques for correcting rain path attenuation are known to be unstable when the total attenuation exceeds few decibels, a relatively common case for intense rainfall at C-band and higher frequencies. This paper uses the iterative correction combined with a neural network and a differential phase constraint to stabilize the attenuation correction procedure. The rationale behind a hybrid approach is to merge the advantage of polarimetric radar measurements to constrain the inverse problem, as done by the self-consistent rain profiling algorithm, within an iterative numerical solution.

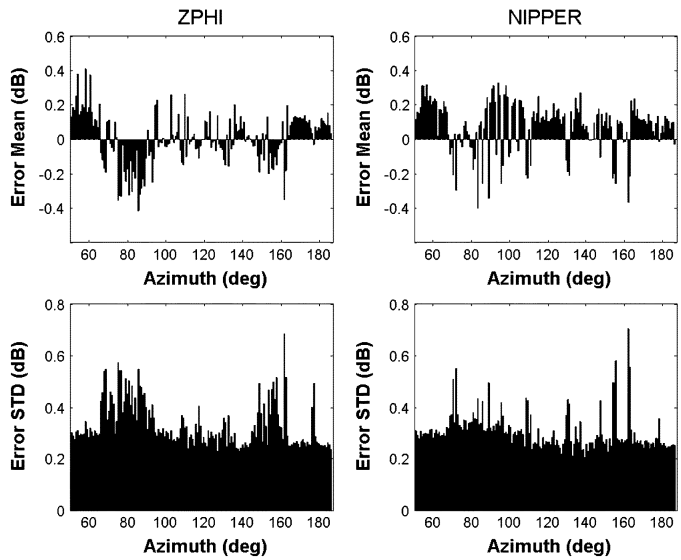

Fig. 8. Differential reflectivity retrieval. The NIPPER performance (right panels) is compared with the rain profiling algorithm one (left panels) in presence of system bias (1dBZ on Z_{hh} and 0.2 dB on Z_{dr}).

A new stable backward iterative technique to correct for path attenuation and differential attenuation is presented. The proposed neural network iterative polarimetric precipitation estimator by radar (NIPPER) is based on a polarimetric model used to train an embedded neural network, constrained by the measurement of the differential phase along the rain path. The adopted polarimetric model is able to simulate amplitude and phase radar response starting from the characterization of raindrop distributions with respect to shape, size, and orientation distribution.

Numerical simulations have been used to investigate the efficiency, accuracy, and robustness of proposed technique. The performances of NIPPER at C-band have been evaluated by using a radar volume scan generated from S-band radar measurements. The latter have been inverted, using a parametric regression algorithm, in order to estimate the raindrop size distribution. Sensitivity analysis has been performed in order to evaluate the expected errors of NIPPER in terms of reconstructed radar observables, taking into account both the error budget and the impact of system bias. These results have shown that NIPPER tends to exhibit a relatively better accuracy and robustness when compared with the self-consistent rain profiling technique.

Acknowledgment

The authors would like to thank M. I. Mishchenko for providing the basic T-Matrix code, used in the scattering calculations. The comments and suggestions of the reviewers are gratefully acknowledged.

References

[1] V. N. Bringi and V. Chandrasekar, *Polarimetric Doppler Weather Radar*. Cambridge, U.K.: Cambridge Univ. Press, 2001.

[2] R. J. Doviak, V. Bringi, A. Ryzhkov, A. Zahrai, and S. S. Zrnić, "Considerations for polarimetric upgrades to operational WSR-88D radars," *J. Atmos. Ocean. Technol.*, vol. 17, pp. 257–278, 2000.

[3] E. Gorgucci, G. Scarchilli, and V. Chandrasekar, "Sensitivity of multiparameter radar rainfall algorithms," *J. Geophys. Res.*, vol. 105, pp. 2215–2223, 2000.

[4] E. Gorgucci, V. Chandrasekar, V. N. Bringi, and G. Scarchilli, "Estimation of raindrop size distribution parameters from polarimetric radar measurements," *J. Atmos. Sci.*, vol. 59, pp. 2373–2384.

[5] T. J. Smyth and A. J. Illingworth, "Correction for attenuation of radar reflectivity using polarization data," *Q. J. R. Meteorol. Soc.*, vol. 124, pp. 2393–2415, 1998.

[6] J. Testud, E. Le Bouar, E. Obligis, and M. Ali-Mehenni, "The rain profiling algorithm applied to polarimetric weather radar," *J. Atmos. Ocean. Technol.*, vol. 17, pp. 332–356, 2000.

[7] E. Le Bouar, J. Testud, and T. D. Keenan, "Validation of the rain profiling algorithm ZPHI from the C-band polarimetric weather radar in Darwin," *J. Atmos. Ocean. Technol.*, vol. 18, pp. 1819–1837, 2001.

[8] V. N. Bringi, T. D. Keenan, and V. Chandrasekar, "Correcting C-band radar reflectivity and differential reflectivity data for rain attenuation: A self-consistent method with constraints," *IEEE Trans. Geosci. Remote Sens.*, vol. 39, no. 9, pp. 1906–1915, Sep. 2001.

[9] V. N. Bringi, V. Chandrasekar, N. Balakrishnan, and D. S. Zrnić, "An examination of propagation effects in rainfall on radar measurements at microwave frequencies," *J. Atmos. Ocean. Technol.*, vol. 7, pp. 829–840, 1990.

[10] J. Hubbert, V. Chandrasekar, and V. Bringi, "Processing and interpretation of coherent dual-polarized radar measurements," *J. Atmos. Ocean. Technol.*, vol. 10, pp. 155–164, 1993.

[11] D. S. Zrnić and A. Ryzhkov, "Advantages of rain measurements using specific differential phase," *J. Atmos. Ocean. Technol.*, vol. 13, pp. 454–464, 1996.

[12] P. H. Hildebrand, "Iterative correction for attenuation of 5 cm radar in rain," *J. Appl. Meteorol.*, vol. 17, pp. 508–514, 1978.

[13] R. Meneghini, "Rain rate estimates for an attenuating radar," *Radio Sci.*, vol. 13, pp. 459–470, 1978.

[14] K. Aydin, Y. Zhao, and T. A. Seliga, "Rain-induced attenuation effects on C-band dual-polarization meteorological radar," *IEEE Trans. Geosci. Remote Sens.*, vol. 27, no. 1, pp. 57–66, Jan. 1989.

[15] E. Gorgucci, G. Scarchilli, and V. Chandrasekar, "Error structrure of radar rainfall measurement at C-band frequencies with dual-polarization algorithm for attenuation correction," *J. Geophys. Res.*, vol. 101, pp. 26 461–26 471, 1996.

[16] W. Hitschfeld and J. Bordan, "Errors inherent in the radar measurement of rainfall at attenuating wavelengths," *J. Meteorol.*, vol. 58–67, 1954.

[17] R. Meneghini, J. Eckerman, and D. Atlas, "Determination of rain rate from spaceborne radar using measurements of total attenuation," *IEEE Trans. Geosci. Remote Sens.*, vol. GE-21, no. 1, pp. 34–43, Jan. 1983.

[18] R. Meneghini and K. Nakamura, "Range profiling of the rain rate by an airborne weather radar," *Remot. Sens. Environ.*, vol. 31, pp. 193–209, 1990.

[19] M. Marzoug and P. Amayenc, "Improved range-profiling algorithm of rainfall rate from a spaceborne radar with path-integrated attenuation constraint," *IEEE Trans. Geosci. Remote Sens.*, vol. 29, no. 4, pp. 584–592, Jul. 1991.

[20] R. Meneghini, T. Kozu, H. Kumagai, and W. C. Boncyk, "A study of rain estimation methods from space using dual-wavelength radar measurements at near-nadir incidence over ocean," *J. Atmos. Ocean. Technol.*, vol. 9, pp. 364–382, 1992.

[21] M. Marzoug and P. Amayenc, "A class of single- and dual-frequency algorithms for rain-rate profiling from spaceborne radar," *J. Atmos. Ocean. Technol.*, vol. 11, pp. 1480–1506, 1994.

[22] T. Iguchi and R. Meneghini, "Intercomparisons of single-frequency methods for retrieving a vertical profile from airborne or spaceborne radar data," *J. Atmos. Ocean. Technol.*, vol. 11, pp. 1507–1516, 1994.

[23] T. Iguchi, T. Kozu, R. Meneghini, J. Awaka, and K. Okamoto, "Rain-profiling algorithm for the TRMM precipitation radar," *J. Appl. Meteorol.*, vol. 39, pp. 2038–2052, 2000.

[24] R. Meneghini, T. Iguchi, T. Kozu, L. Liao, K. Okamoto, J. A. Jones, and J. Kwiatkowski, "Use of the surface reference technique for the path attenuation estimates from the TRMM precipitation radar," *J. Appl. Meteorol.*, vol. 39, pp. 2053–2070, 2000.

[25] A. R. Jameson, "The effect of temperature on attenuation-correction schemes in rain using polarization propagation differential phase shift," *J. Appl. Meteorol.*, vol. 31, pp. 1106–1118, 1992.

[26] J. Hubbert and V. Bringi, "An iterative filtering technique for the analysis of copolar differential phase and dual-frequency radar measurements," *J. Atmos. Ocean. Technol.*, vol. 15, pp. 643–648, 1995.

[27] F. S. Marzano, E. Picciotti, and G. Vulpiani, "Rain field and reflectivity vertical profile reconstruction from C-band radar volumetric data," *IEEE Trans. Geosci. Remote Sens.*, vol. 42, no. 5, pp. 1033–1046, May 2004.

[28] G. Vulpiani, E. Picciotti, G. Ferrauto, and F. S. Marzano, "Sensitivity analysis of self-consistent polarimetric rain retrieval to C-band radar observables," in *Proc. IGARSS*, vol. 2, Toulouse, France, Jul. 21–15, 2003, pp. 1160–1162.

[29] R. J. Doviak and D. S. Zrnić, *Doppler Radar and Weather Observations*, 2nd ed. San Diego, CA: Academic, 1993.

[30] J. S. Marshall and W. M. K. Palmer, "The distribution of rain-drops with size," *J. Meteorol.*, vol. 5, pp. 165–166, 1948.

[31] R. S. Sekon and R. C. Srivastava, "Doppler radar observations of drop size distribution in a thunderstorm," *J. Atmos. Sci.*, vol. 28, pp. 983–994, 1971.

[32] V. Chandrasekar and V. N. Bringi, "Simulation of radar reflectivity and surface measurements of rainfall," *J. Atmos. Oceanic Technol.*, vol. 4, pp. 464–478, 1987.

[33] J. Testud, S. Oury, R. A. Black, P. Amayenc, and X. Dou, "The concept of "normalized" distribution to describe raindrop spectra: A tool for cloud physics and cloud remote sensing," *J. Appl. Meteorol.*, vol. 40, pp. 1118–1140, 2001.

[34] A. J. Illingworth and T. M. Blackman, "The need to represent raindrop size spectra as normalized gamma distributions for the interpretation of polarization radar observations," *J. Appl. Meteorol.*, vol. 41, pp. 1578–1583, 2002.

[35] C. Chuang and K. V. Beard, "A numerical model for the equilibrium shape of electrified raindrops," *J. Atmos. Sci.*, vol. 19, pp. 1374–1389, 1990.

[36] K. V. Beard and A. R. Jameson, "Raindrop canting," *J. Atmos. Sci.*, vol. 40, pp. 448–454, 1983.

[37] M. I. Mishchenko, "Light scattering by randomly oriented axially symmetric particles," *J. Opt. Soc. Amer. A*, vol. 8, pp. 871–882, 1991.

[38] ——, "Calculation of the amplitude matrix for a nonspherical particle in a fixed orientation," *Appl. Opt.*, vol. 39, pp. 1026–1031, 2000.

[39] ——, *Light Scattering by Nonspherical Particles*. Orlando, FL: Academic, 2000.

[40] P. S. Ray, "Broadband complex refractive indexes of ice and water," *Appl. Opt.*, vol. 11, pp. 1836–1844, 1972.

[41] D. Atlas and C. W. Ulbrich, "Path- and area-integrated rainfall measurement by microwave attenuation at 1–3 cm band," *J. Appl. Meteorol.*, vol. 16, pp. 1322–1331, 1977.

[42] G. Vulpiani, E. Picciotti, G. Ferrauto, F. S. Marzano, and V. Chandrasekar, "C-band dual polarization observation of rainfall: Application of an iterative approach with embedded neural network," presented at the *3rd ERAD Conf.*, Visby, Sweden, Sep. 6–10, 2004.

[43] G. Vulpiani, F. S. Marzano, and V. Chandrasekar, "Model-based iterative approach to polarimetric radar rainfall estimation in presence of path attenuation," *Adv. Geosci.*, vol. 2, pp. 51–57, 2005.

[44] M. Abramowitz and I. A. Stegun, Eds., *Handbook of Mathematical Functions with Formulas, Graphs, and Mathematical Tables, 9th printing*. New York: Dover, 1972.

[45] G. Scarchilli, E. Gorgucci, V. Chandrasekar, and T. A. Seliga, "Rainfall estimation using polarimetric techniques at C-band frequencies," *J. Appl. Meteorol.*, vol. 32, pp. 1150–1160, 1993.

[46] V. Chandrasekar, E. Gorgucci, and G. Scharchilli, "Optimization of multiparameter radar estimates of rainfall," *J. Appl. Meteorol.*, vol. 12, pp. 1288–1293, 1993.

[47] E. Gorgucci, G. Scharchilli, and V. Chandrasekar, "A procedure to calibrate multiparameter weather radar using properties of the rain medium," *IEEE Trans. Geosci. Remote Sens.*, vol. 37, no. 1, pp. 269–276, Jan. 1999.

[48] S. Haykin, *Neural Networks: A Comprehensive Foundation*. New York: Macmillan, 1995.

[49] F. S. Marzano and P. Bauer, "Sensitivity analysis of airborne microwave retrieval of stratiform precipitation to the melting layer parameterization," *IEEE Trans. Geosci. Remote Sens.*, vol. 39, no. 1, pp. 75–91, Jan. 2001.

Gianfranco Vulpiani received the laurea and Ph.D. degrees in physics from the University of L'Aquila, L'Aquila, Italy, in 2001 and 2005, respectively.

In 2001, he joined the Department of Physics and the Center of Excellence (CETEMPS), University of L'Aquila as a Research Scientist on ground-based radar meteorology, with a special focus on C-band applications. In 2004, he was a Visiting Student at the Colorado State University (CSU). His current research concerns active remote sensing of the atmosphere from ground-based sensors, with a particular focus on development of polarimetric precipitation retrieval techniques.

Frank Silvio Marzano (S'89–M'99–SM'03) received the laurea degree (cum laude) in electrical engineering and the Ph.D. degree in applied electromagnetics, in 1988 and 1993, respectively, both from the University of Rome "La Sapienza," Rome, Italy.

He has been with the Department of Electronic Engineering, University "La Sapienza."He currently teaches courses on antennas, propagation, and remote sensing. In 1993, he collaborated with the Institute of Atmospheric Physics (CNR), Rome. From 1994 until 1996, he was with the Italian Space Agency, Rome, as a Post-Doctorate Researcher. After being a Lecturer at the University of Perugia, Perugia, Italy, in 1997, he joined the Department of Electrical Engineering, University of L'Aquila. His current research interests are passive and active remote sensing of the atmosphere from ground-based, airborne, and spaceborne platforms, with a particular focus on precipitation using microwave and infrared data, development of inversion methods, radiative transfer modeling of scattering media, and radar meteorology issues. He is also involved in radiopropagation topics in relation to incoherent wave modeling, scintillation prediction, and rain fading analysis along satellite microwave links. He has published more than 45 papers in refereed international journals and books and more than 170 extended abstract in international and national congress proceedings.

Dr. Marzano received the Young Scientist Award of the XXIV General Assembly of the International Union of Radio Science in 1993. In 1998, he was the recipient of the Alan Berman Publication Award from the Naval Research Laboratory, Washington, DC. Since 2001, he is the Italian National Delegate for the European COST actions number 720 on meteorological remote sensing and number 280 on satellite communications. He is an Associate Editor for IEEE GEOSCIENCE AND REMOTE SENSING LETTERS. In 2004, he was Co-Guest Editor of the special issue on MicroRad04 for IEEE TRANSACTIONS ON GEOSCIENCE AND REMOTE SENSING.

V. Chandrasekar (S'83–M'87–F'03) is currently a Professor at Colorado State University (CSU), Fort Collins. He has been involved with research and development of weather radar systems for over 20 years and has about 25 years of experience in radar systems. He has played a key role in developing the CSU-CHILL National Radar Facility as one of the most advanced meteorological radar systems available for research, and continues to work actively with the CSU-CHILL radar supporting its research and education mission and is a Co-PI of the facility. In addition, he also serves as the Deputy Director of the recently established NSF-ERC, Center for Collaborative Adaptive Sensing of the Atmosphere. He is an avid experimentalist conducting special experiments to collect *in situ* observations to verify the new techniques and technologies. He is coauthor of two textbooks, *Polarimetric and Doppler Weather Radar* (Cambridge, U.K.: Cambridge Univ. Press) and *Probability and Random Processes* (New York: McGraw-Hill). He has served as academic advisor for over 40 graduate students.

Dr. Chandrasekar has served as a member of the National Academy of Sciences Committee on "Weather Radar Technology beyond NEXRAD" and is the General Co-Chair for the IGARSS'06 Symposium. He has received numerous awards including the Abell Foundation Outstanding Researcher Award, Outstanding Advisor Award, as well as the Distinguished Diversity Services Award.

Sanghun Lim received the B.A. degree from Yonsei University, Seoul, Korea, and the M.S. degree from the Colorado State University, Fort Collins, both in electrical engineering. He is currently pursuing the Ph.D. degree at Colorado State University.

His research interests include hydrometeor classification using dual-polarization radar measurements and attenuation correction with/without dual-polarization and networked radar systems.